Electrochimica Acta 297 (2019) 398–405

Contents lists available at ScienceDirect

Electrochimica Acta

journal homepage: www.elsevier.com/locate/electacta

Improving the electrochemical performance of $LiNi_{1/3}Co_{1/3}Mn_{1/3}O_2$ cathode material via tungsten modification

Bi Luo [a], Bing Jiang [a, *], Peng Peng [a], JiaJia Huang [b], Jiewei Chen [a], Meicheng Li [a], Lihua Chu [a], Yingfeng Li [a]

[a] State Key Laboratory of Alternate Electrical Power System with Renewable Energy Sources, School of Renewable Energy, North China Electric Power University, Beijing 102206, China
[b] Research and Development Center, CITIC Guoan MGL Power Source Technology Co., Ltd, 18 Baifuquan Rd. Changping, Beijing, 102200, China

ARTICLE INFO

Article history:
Received 21 August 2018
Received in revised form
22 November 2018
Accepted 28 November 2018
Available online 29 November 2018

Keywords:
$LiNi_{1/3}Co_{1/3}Mn_{1/3}O_2$
Tungsten compound
Surface modification
Lithium-ion battery

ABSTRACT

Poor rate capability and capacity degradation of $LiNi_xCo_yMn_zO_2$ restricts its practical commercial applications at high operating voltage (>4.3 V). $LiNi_{1/3}Co_{1/3}Mn_{1/3}O_2$ is successfully modified by tungsten compound through a cost-effective ball-milling and annealing process. The rate capability of W-modified cathode is increased by 57.6% at 10C in 3.0–4.5 V. Moreover, after 100 cycles the capacity retention is improved from 80% to 96% under 0.5C. At 1C, W-modified cathode still maintains 145 mAh g^{-1} discharge capacity after 100 cycles, which has 16% increase than pristine $LiNi_{1/3}Co_{1/3}Mn_{1/3}O_2$. The improvements on rate and cycle performance are introduced by enhanced Li-ion diffusion and surface stability by tungsten modification.

1. Introduction

The wide applications in the large-scale energy storage devices and electronics, more researches focus on the high capacity, larger energy density and longer life Li-ion battery [1–11]. As the earliest commercialized cathode material, $LiCoO_2$ can't meet the increasing practical demand due to its low practical capacity, higher cost of cobalt and unreliable safety. $LiNi_xCo_yMn_zO_2$ (NMC; $0 \leq x, y, z < 1$) is pioneered by Ohzuku's [12] and Dahn's [13] groups, in which the properties depend on the ratio of transition-metal elements in the structure. Compared with $LiNiO_2$, $LiCoO_2$ and $LiMnO_2$, NMC has more advantages including satisfactory capacity, better cycle property, more stable structure and lower cost, which has been recently used as cathode of Lithium-ion battery [14,15]. In NMC micro-structures, Ni delivers capacity, Co improves the rate performance, and Mn maintains the structural stability. Though NMC is usually charged to a voltage of 4.3 V, the charge cut-off potential of NMC can be increased to a higher voltage (4.5 V) in order to get more capacity. However, the severe capacity degradation is aggravated because of the NMC/electrolyte interfacial reactions during high cut-off voltage cycling. For example, the $LiPF_6$ can react with moisture residues in electrolyte to produce HF, which damages the NMC and decreases the electrochemical performance. Additionally, the high cut-off voltage can accelerate the dissolution of transition metals and structural degradation of NMC because of the interfacial reactions between highly delithiated NMC and electrolyte. Therefore, the NMC cathode is restricted in practical commercial applications due to its significant degradation of the cycling stability and rate capability during high cut-off voltage cycling [6,16–18].

Many surface modification methods were proposed to improve the electrochemical property of cathodes. Researchers found that coating layers of metallic oxide [19–21], fluoride [22,23], phosphate [24,25] can suppressed interfacial reactions to increase the electrochemical property of NMC. Particularly, some metallic oxides could effectively scavenge the HF that resulting from the side reactions between moisture residues and $LiPF_6$. Yang [26] reported that the enhanced cycling stability and thermal stability was attributed to the fact that Al_2O_3 suppressed interfacial reactions and inhibited oxygen release. Zhang [27] improved the stability and capacity of $Li(Ni_{0.5}Co_{0.2}Mn_{0.3})O_2$ using Mo-doping and Mo-coating, which could reduce the cation mixing and impede the interfacial reactions between NMC and electrolyte. Similar to other metal oxides coating layers, tungsten oxide also can react with HF, and remain its stable electrochemical properties during charging/

* Corresponding author.
E-mail address: Bingjiang@ncepu.edu.cn (B. Jiang).

https://doi.org/10.1016/j.electacta.2018.11.202
0013-4686/

discharging process of NMC [28,29]. Furthermore, Aykol [30] developed a high-throughput density functional theory based framework to optimize coating materials for layered cathodes in Li-ion batteries. According to the report, tungsten oxide is an optimal coating for layered cathodes due to its advantages in thermodynamic stability, electrochemical stability and the reactivity with HF. Additionally, according to previous reports [31,32], the tungsten compounds as like lithium tungstate also can be used to modify the cathode materials, which can improve the lithium-ion diffusion and reduce the interfacial resistance of $LiCoO_2$. From previous studies, the tungsten may be an effective material system for NMC cathode modification.

In this study, tungsten-modified $LiNi_{1/3}Co_{1/3}Mn_{1/3}O_2$ particle was synthesized by a facile cost-effective ball-milling and annealing process. This modification method can reduce the residual lithium compounds and form tungsten compounds like tungsten oxide and lithium tungstate, which can retard the cathode/electrolyte interfacial reactions and facilitate Li-ion diffusion in the batteries. After modification, the cycle and rate performance of NMC cathode batteries under 3.0–4.5 V are improved significantly. Furthermore, Li-ion diffusion is investigated to reveal the inertial mechanism of tungsten modification on cathode performance.

2. Experiment details

2.1. Materials

$LiNi_{1/3}Co_{1/3}Mn_{1/3}O_2$ (NMC) powder was prepared by coprecipitation method [33,34]. The aqueous solution of $NiSO_4$, $CoSO_4$, and $MnSO_4$ with a concentration of 2M was continuously stirring. Then, 2M Na_2CO_3 solution with 0.2 M NH_4OH was also added into the beaker. The precipitates $(Ni_{1/3}Co_{1/3}Mn_{1/3})CO_3$ powders were washed by water, and dried at 80 °C. After that, dried powders were mixed with Li_2CO_3 and calcinated at 850 °C for 16 h. The exact molar ratio between Li_2CO_3 and $(Ni_{1/3}Co_{1/3}Mn_{1/3})CO_3$ was 0.51.

The different mass ratios of $(NH_4)_2WO_4$ (Alfa Aesar, 99.99%) was added to pristine $LiNi_{1/3}Co_{1/3}Mn_{1/3}O_2$, and then was dispersed in acetone. The mixture was in ball-milling with a speed of 300 rpm for duration of 20 min followed by a 10 min resting interval. This milling process was repeated for 3 times. After dried at around 80 °C for 4 h, the mixture was calcined at 800 °C for 4 h, and then cooled naturally. Finally, the samples of W-modified NMC (2, 3, and 4 wt% W) were prepared, and were denoted here after as NMC-2% W, NMC-3%W, NMC-4%W. As a reference, NMC-annealed samples were prepared with the same ball milling and annealing process as that described above but without adding $(NH_4)_2WO_4$.

2.2. Material characterization

The cathode materials were represented by X-ray diffraction (XRD, BRUKER, D8 Focus, Germany) using the Cu-Ka radiation with 10–80° incidence angle. The morphology of the cathode materials was investigated using scanning electron microscope (SEM, Hitachi SU8010) with collecting energy disperse X-ray spectroscopy (EDS) maps and transmission electron microscope (TEM, Tecnai G2 F20). The element compositions information of as-prepared samples were obtained by inductively coupled plasma-optical emission spectroscopy (ICP-OES, Agilent 730). X-ray photoelectron spectrum (XPS) was used to analysis the surface element valence state and constituents by ESCALAB 250Xi X-ray photoelectron spectroscope (Al Kα radiation).

2.3. Electrochemical measurements

As cathode materials, the pristine and W-modified NMC were mixed with acetylene black (Super-P) and polyvinylidene fluoride (PVDF) (8:1:1) in N-methyl-2-pyrrolidinone (NMP). Subsequently, the cathode slurry coated on the aluminum foil was vacuum dried at 110 °C for 10 h. CR2032-type coin half-cell was assembled in Ar-filled glove box (both H_2O and $O_2 < 0.1$ ppm). The device was composed by the as-prepared cathode electrode, anode (Li metal), separator (glass fiber, Whatman), and electrolyte (1M $LiPF_6$/EC-DMC). Cyclic voltammetry (CV) tests were conducted by electrochemical workstation (CHI660e, Shanghai Chenhua). The half-cells were galvanostatically charged and discharged using the various current density (1C is 180 mA g^{-1}) in 3.0–4.5 V vs Li/Li^+ using the multichannel battery test system (Land, China). An electrochemical impedance spectrum (EIS) was recorded with the electrochemical workstation (Zahner Zennium) under 10 mV and a 100 kHz to 0.01 Hz range [35,36].

3. Results and discussion

3.1. Morphology characterization of cathode materials

Fig. 1 shows the structural information of pristine NMC and W-modified samples by XRD. The main peaks of all samples are well indexed with a typical α-$NaFeO_2$ structure [8,37–40]. Highly ordered layered structure of NMC and W-modified samples are reflected by these obvious peaks and peak splits of (006)/(102) and (018)/(110) [7,41,42]. XRD spectra of the samples indicate that the crystal structure of NMC is not changed by annealing process or the coating layers.

Fig. 2 shows the surface morphology of NMC and NMC-3%W samples. Both the samples of NMC and NMC-3%W keep the secondary spherical-like particle well with a size of about 9–13 μm, and the surface is not obviously changed by W modification. In addition, the EDS-mappings of NMC-3%W sample in Fig. 2(d) indicate that W element has been modified successfully on the surface of NMC [27]. Besides, the detailed W contents of NMC and W-modified samples detected by ICP-OES were shown in Table S2.

The particles of NMC and NMC-3%W are also observed by TEM, as shown in Fig. 3. The measured inter-planar distances are 0.47 nm and 0.23 nm in the crystallized areas, which match well to the (003) and (012) crystal planes of NMC. From Fig. 3(b), an approximate 5 nm-thick layer is observed on the surface of NMC. The ammonium tungsten oxide can not only react with the residual lithium like LiOH (in Eq. (1)) and Li_2CO_3 [43,44], but also decompose into WO_3 [45] (in Eq. (2)). Therefore, it is supposed that this amorphous

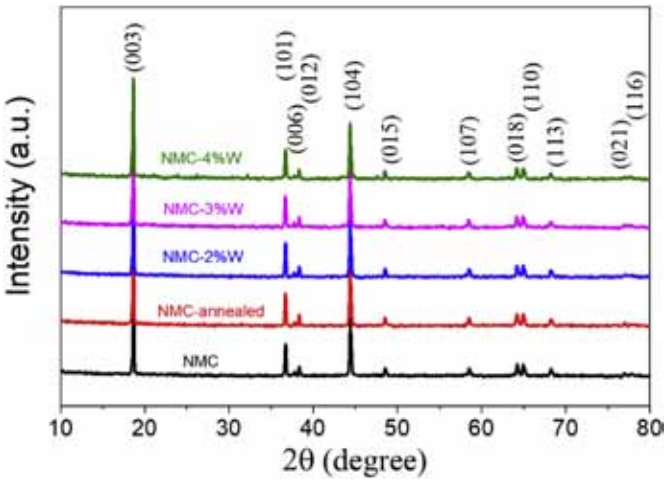

Fig. 1. X-ray diffraction data of pristine NMC, NMC-annealed and W-modified samples.

film may be consist of WO_3 or the compounds of Li, W and O.

$$(NH_4)_2WO_4 + 2LiOH \rightarrow Li_2WO_4 + 2NH_3 + 2H_2O \quad (1)$$

$$(NH_4)_2WO_4 \rightarrow WO_3 + 2NH_3 + H_2O \quad (2)$$

XPS spectra of W 4f and O1s of pristine NMC and NMC-3%W samples are given in Fig. 4. From the fitting results in Fig. 4(a), four peaks of W 4f and one peak of W 5p can be seen in the NMC-3% W sample, whereas there is no peak of W 4f or W 5p in the pristine NMC sample. The peaks at 37.4 and 35.3 eV corresponding to W 4f5/2 and W 4f7/2 are ascribed to W^{6+}, whereas the peaks at 37.0 and 34.9 eV corresponding to W 4f5/2 and W 4f7/2 represented W^{5+} [20,21,46]. It is supposed that some W^{6+} were reduced to W^{5+} by inserting Li^+ [47] or transition metal ion (Ni^{2+} or Mn^{4+}) [21]. The XPS results indicate the presence of tungsten compound in the NMC-3%W samples. Meanwhile, the change of O 1s peaks in Fig. 4(b) suggests that the oxygen environment on NMC surface is changed by tungsten compound. Compare with the pristine NMC sample, the lower intensity of peak 529.5 eV and higher intensity of peak 531.4 eV suggest that there are more O^{2-} from tungsten compound. Moreover, there is no obvious change of the Ni 2p, Co 2p, and Mn 2p spectra (in Fig. S1), which indicate that the valence states of Ni, Co and Mn are corresponding to 2+, 3 + and 4+, respectively [48]. Overall, all above results confirm that tungsten compound has successfully been modified on NMC particles.

3.2. Electrochemical performance

The cyclic voltammetry (CV) of the first ten cycles were conducted in the range of 3.0 and 4.5 V, as shown in Fig. 5(a and b). On one hand, the only one pair of cathodic/anodic peaks around 3.8 V from redox process of Ni^{2+}/Ni^{4+} [49,50], are both observed for pristine NMC and NMC-3%W during charge/discharge. On the other hand, there are no cathodic/anodic peaks corresponding to the redox process of WO_3 indicating that the coating layer is electrochemically stable, which are in accord with the calculation results [30]. Moreover, for pristine NMC, the oxidation/reduction peaks move to high/low potential and diminish in intensity after 10 cycles. Compared with the pristine NMC, the curves of NMC-3%W have a relatively smaller shift in redox peaks, which are attributed to the tungsten compounds between NMC surface and electrolyte. During cycling, the tungsten compound can retards the cathode/electrolyte interfacial reactions and reduces the surface degradation, which can reduce the potential shift and intensity attenuation. The data of the redox peaks of pristine NMC and NMC-3%W electrodes in first, fifth and tenth scans are compared in Table 1. For the pristine NMC, with the scan cycles increasing, the potential difference between anodic and cathodic peaks is increasing. The potential difference is 0.123 V in the first cycle, 0.125 V in the fifth cycle, and 0.153 V in the tenth cycle. However, for the NMC-3%W electrodes, the potential difference is 0.111 V in the first cycle, only 0.046 V in the fifth cycle, and 0.042 V in the tenth cycle. The smaller potential difference between redox peaks in NMC-3%W electrodes is attributed to the lower electrochemical polarization and faster Li-ion diffusion during redox process of Ni^{2+}/Ni^{4+}.

The galvanostatic charge-discharge cycling experiments were performed under 3.0–4.5 V range. The rate property of NMC and W-modified NMC is shown in Fig. 6 (a). With the current density increasing, the specific capacity of all samples reduce, which is attributed to an electrochemical polarization. When current density returns to 0.1C again, the capacities of the W-modified NMC are closer to their initial capacities at 0.1C than that of the pristine NMC samples. This result indicates that the capacity degradation during high rate cycling is reduced by tungsten modification. From Fig. 6 (a), it is found that rate capability of NMC-3%W samples have an improvement compared with pristine NMC. The discharge capacities of the pristine NMC samples are about 170, 165, 152, 137, 128, 105, 78 and 160 mAh g^{-1} corresponding to 0.1C, 0.2C, 0.5C, 1C, 2C,

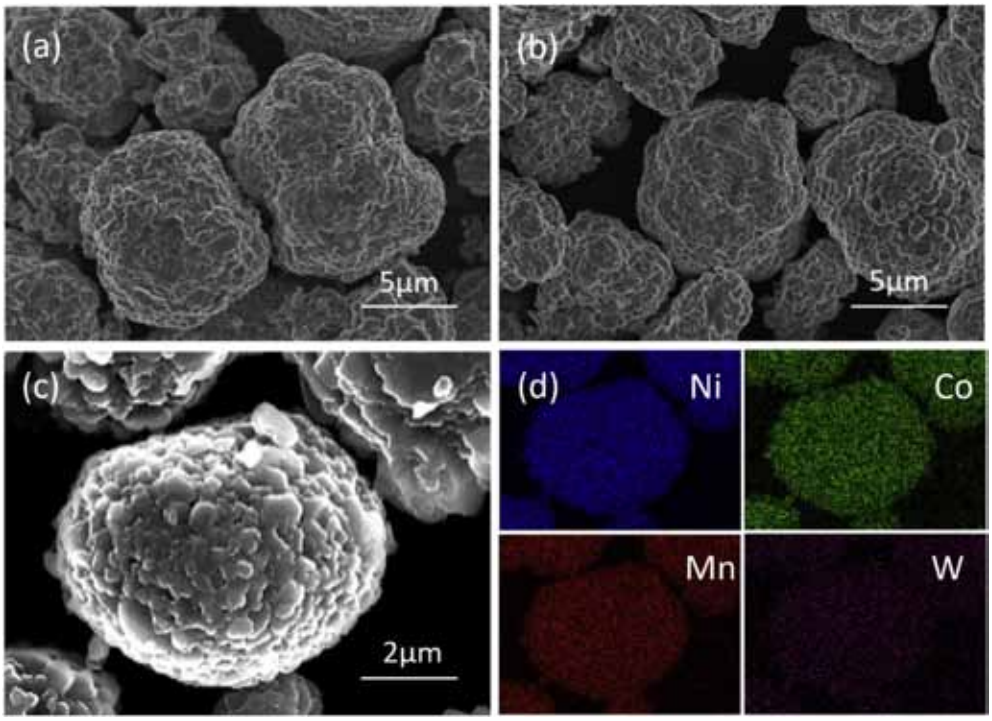

Fig. 2. SEM morphology of (a) pristine NMC particles; (b–c) NMC-3%W particles under different magnification; (d) EDS-mapping of NMC-3%W particles.

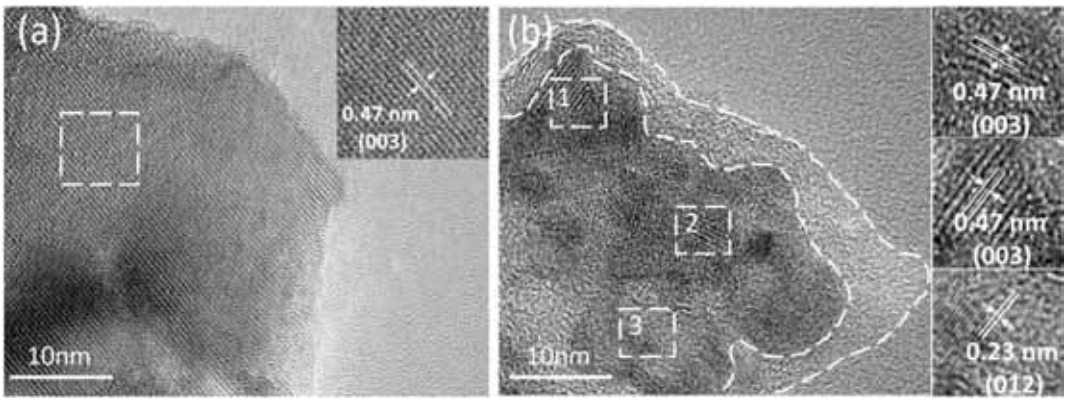

Fig. 3. The HR-TEM images of (a) pristine NMC particle, (b) NMC-3%W sample particle.

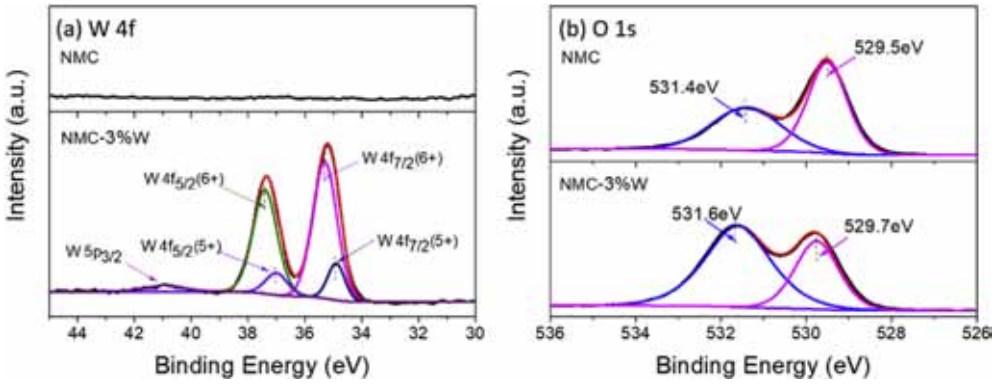

Fig. 4. The XPS spectra of (a) W 4f, (b) O1s for pristine NMC and NMC-3%W samples.

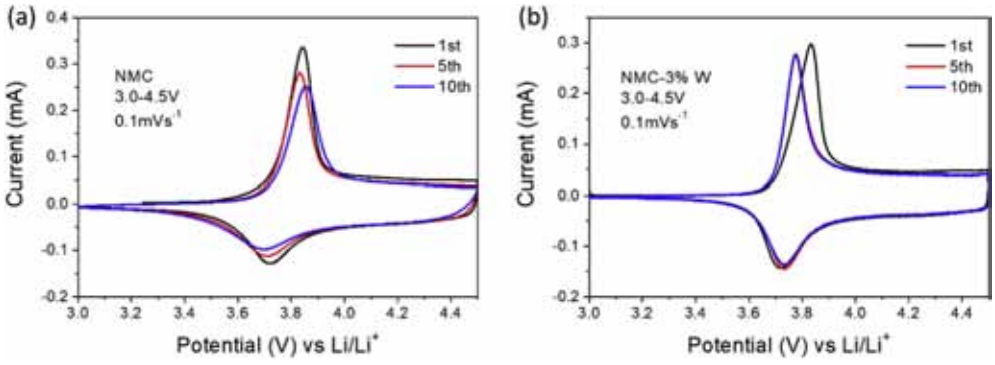

Fig. 5. Cyclic voltammetry profiles of (a) pristine NMC; (b) NMC-3%W in 3.0–4.5 V range with 0.1 mV s^{-1} sweep rate.

Table 1
The potentials of the redox peaks of NCM and NCM-3%W electrodes in the 1st, 5th and 10th scans.

Potential	pristine NCM			NCM-3%W		
	1st	5th	10th	1st	5th	10th
Anodic peak (V)	3.844	3.834	3.854	3.831	3.774	3.775
Cathodic peak (V)	3.721	3.709	3.701	3.720	3.732	3.729
Difference (V)	0.123	0.125	0.153	0.111	0.042	0.046

5C, 10C and 0.1C (again), respectively. While the discharge capacities of NMC-3%W samples are increased to 183, 179, 164, 158, 149, 138, 123 and 177 mAh g^{-1} under the same conditions. Especially at 10C, the value is higher 57.6% than that of pristine NMC. Fig. 6(b and c) show the charge-discharge curves of NMC and NMC-3%W from the rate cycling. Obviously, NMC-3%W samples have lower electrochemical polarization and a more stable voltage plateaus within the range of 3.6–3.9 V at the high rate cycling.

The cycling stability at 0.5C and 1C rates are also enhanced after modification, as shown in Fig. S2 and Fig. 6 (d). For the pristine NMC samples, the discharge specific capacity at 0.5C after 100th cycles is 145 mAh g^{-1} similar to previous literature [51,52]. In addition, the cycling performance of NMC-annealed samples is parallel to the pristine NMC samples, which indicates that the only annealing process has no improvement to the NMC. After modification, the NMC-(2%, 3%, 4%)W samples display enhanced discharge capacities

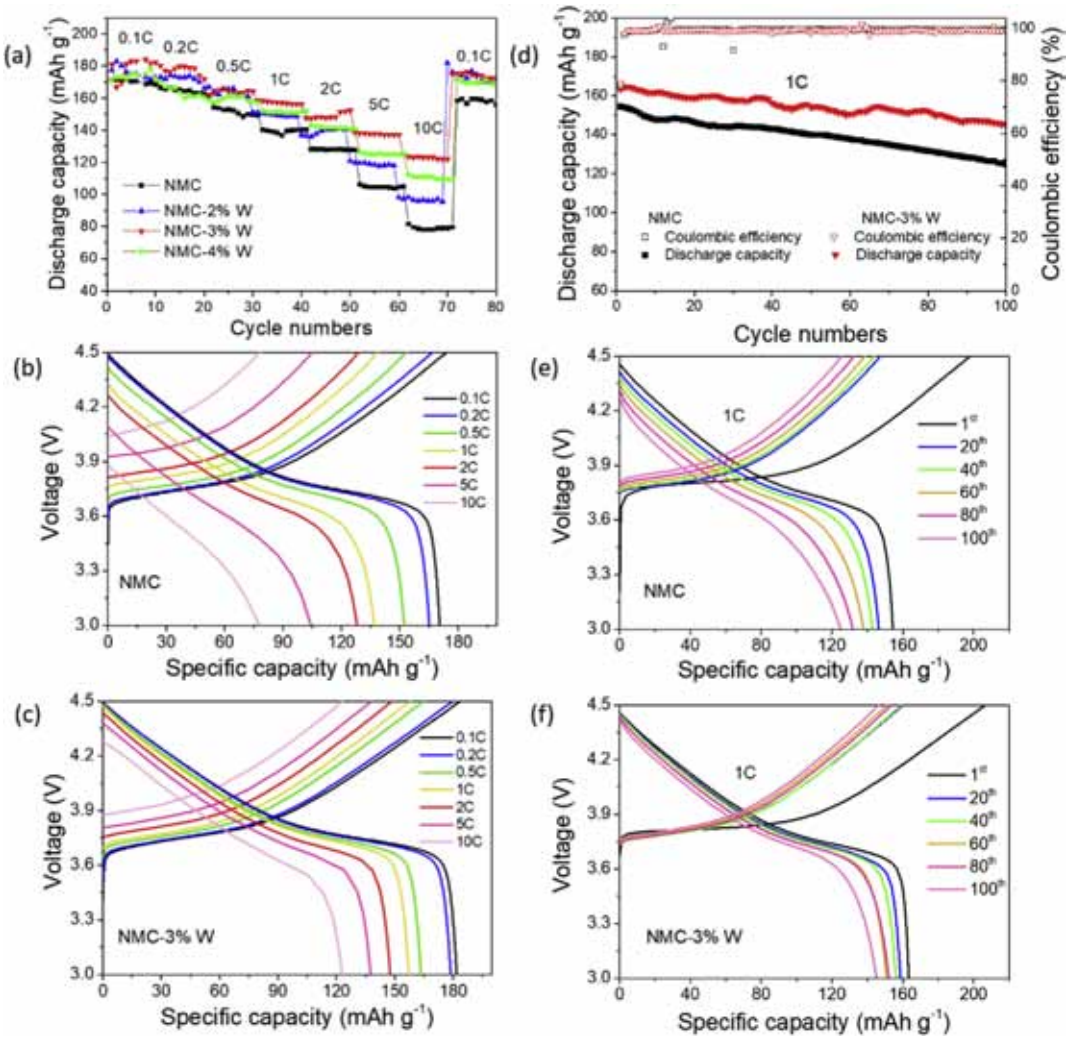

Fig. 6. The electrochemical properties of pristine NMC and NMC-3%W sample. (a) rate performance; (b–c) voltage profiles at different current densities; (d) cycle performance at 1C; (e–f) charge-discharge curves at different cycles.

of 158, 162, 157 mAh g^{-1}, respectively. Therefore, the capacity retention is increased from 80% of pristine NMC to 96% of NMC-3% W sample. Moreover, Fig. 6 (d) is the cycling performance at the rate of 1C in 3.0–4.5 V range. The NMC-3%W samples maintain 145 mAh g^{-1} after 100th cycles, which has 16% increase than pristine NMC sample. It is supposed that this improvement is related to the decrease of interfacial reactions and better surface stability due to the scavenging effect of WO_3 on HF. Fig. 6(e and f) show the voltage versus capacity curves of charge-discharge process at 1C rate for pristine NMC and NMC-3%W samples. With the cycle numbers increasing, the NMC-3%W sample has smaller voltage drops than the pristine NMC in the cycling, which implies a smaller degradation and polarization during cycling. After 100 cycles, the pristine NMC sample has a voltage drop at 0.23 V, while the NMC-3%W sample only has a 0.08 V drop (see Table 2). Overall, NMC-3% W samples obtain better rate and cycling property at high operating voltage.

CV measurements [53] and galvanostatic intermittent titration technique (GITT) [54] methods were used to study the Li-ion diffusion property of pristine NMC electrodes and NMC-3%W electrodes. CVs were performed in 3.0–4.5 V under 0.1–1.0 mV s^{-1} sweep rates, as shown in Fig. 7(a) and (b). With increase of scan rates, the peak currents (I_p) are increasing gradually, while the oxidation (reduction) peak moves to the higher (lower) potential. The obvious shift of redox peak may be ascribed to the increase of electrochemical polarization with CV sweep rate (v). Compared with pristine NMC electrodes, NMC-3%W electrodes have the higher peak currents and lower overpotential, which indicates electrochemical polarization is reduced by tungsten compound. According to previous report [55], the relationship between I_p and $v^{1/2}$ can be described to Eq. (3).

$$I_p = 2.69 \times 10^5 \times n^{3/2} A D^{1/2} v^{1/2} C \quad (3)$$

Where n is charge-transfer number in reactions, A is the electrode area in cm^2, D is Li^+ diffusion coefficient in cm^2 s^{-1}, ν is CV sweep rate in V s^{-1}, and C is Li^+ concentration during the cathode related reactions.

Table 2
Comparison of voltage drop at the beginning of discharging for NCM and NCM-3%W electrodes.

Cycle	1st	20th	40th	60th	80th	100th
NCM	0.04	0.09	0.12	0.15	0.19	0.23
NCM-3%W	0.04	0.04	0.05	0.06	0.06	0.08

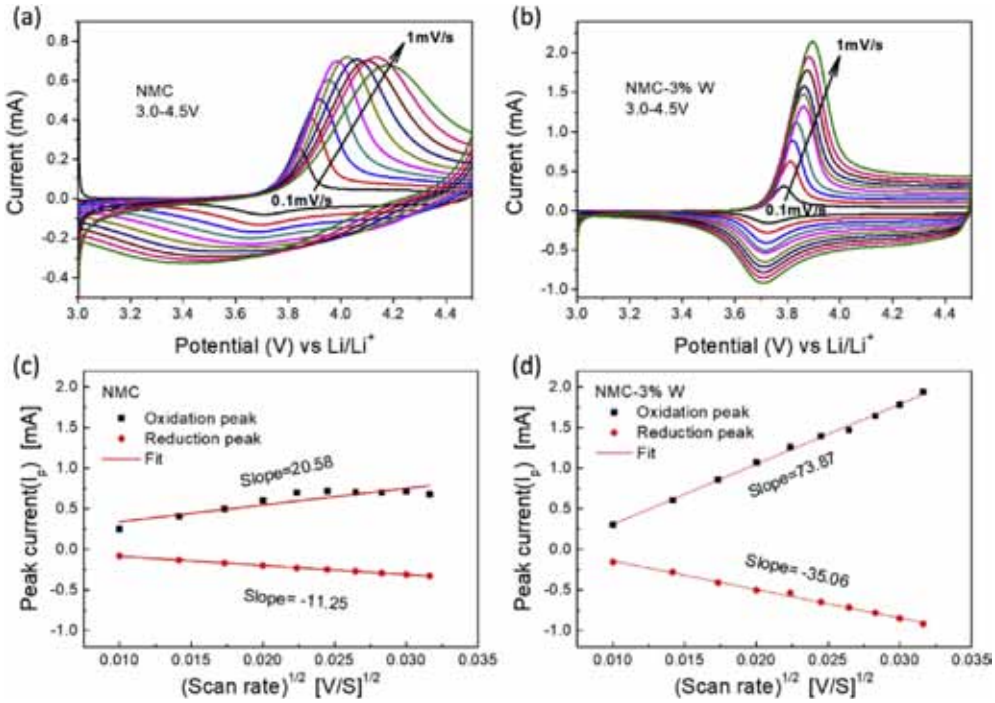

Fig. 7. Estimation Li-ion diffusion coefficient of pristine NMC and NMC-3%W. (a–b) CVs at various sweep rates; (c–d) slopes of redox peaks currents from CVs vs. a square root function of sweep rates.

According to Eq. (1), Li-ion diffusion coefficient (D) can be calculated by the slope of I_p vs. $v^{1/2}$ plots. Therefore, the slope of oxidation peak and reduction peak is given in Fig. 7(c and d). Obviously, the slope of NMC-3%W electrode is bigger than NMC electrode whether for oxidation peak or for reduction peak. The diffusion coefficients for oxidation and reduction process in NMC-3%W electrode are calculated to be $1.76 \times 10^{-10}\,cm^2\,s^{-1}$ and $3.96 \times 10^{-10}\,cm^2\,s^{-1}$, respectively, while diffusion coefficients in NMC electrode are $1.37 \times 10^{-11}\,cm^2\,s^{-1}$ and $4.08 \times 10^{-12}\,cm^2\,s^{-1}$, respectively. Additionally, GITT method also was used to calculate the Li-ion diffusion coefficient, as shown in Fig. S3. During the charge process, the diffusion coefficient of NMC-3%W electrode is about $1.1 \times 10^{-10}\,cm^2\,s^{-1}$, whereas that of pristine NMC electrode is about $3 \times 10^{-11}\,cm^2\,s^{-1}$. According to the diffusion coefficients

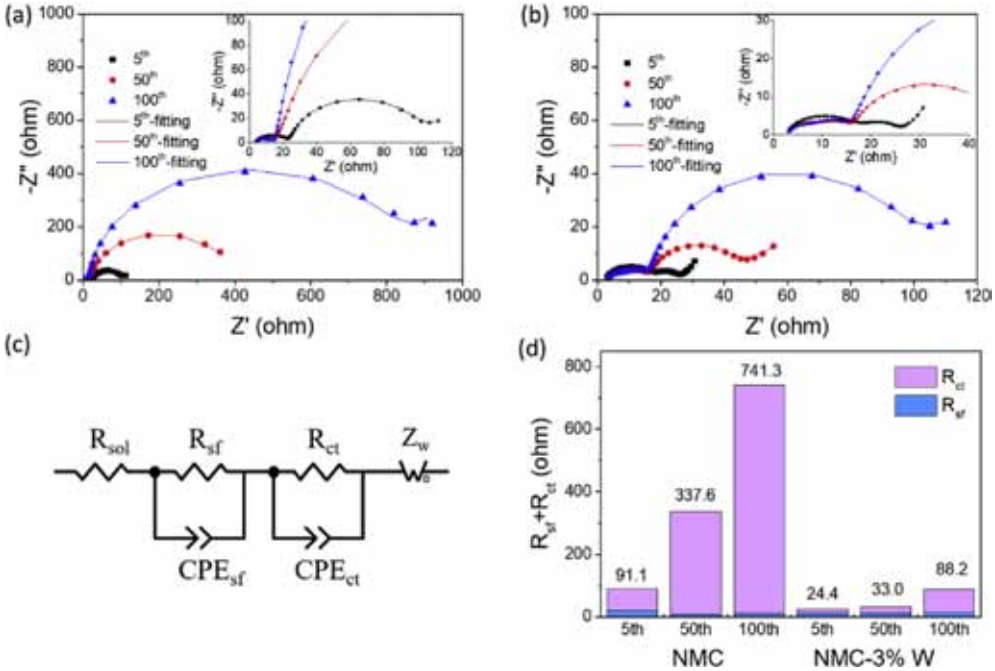

Fig. 8. EIS results of pristine NMC and NMC-3%W. (a–b) Nyquist plots at charging to 4.5 V for 5th, 50th, 100th cycles; (c) Equivalent circuit model for EIS fitting; (d) $R_{sf} + R_{ct}$ in pristine NMC and NMC-3%W.

Table 3
Impedance parameters of pristine NCM and NCM-3%W charging to 4.5 V for 5th, 50th, 100th cycles.

Cycle number	NCM			NCM-3%W		
	R_{sol} (Ω)	R_{sf} (Ω)	R_{ct} (Ω)	R_{sol} (Ω)	R_{sf} (Ω)	R_{ct} (Ω)
5th	3.35	20.09	71.01	2.60	12.86	11.54
50th	2.92	9.06	328.50	2.13	12.63	20.36
100th	3.31	10.32	731.00	2.24	14.93	73.27

calculated by CV and GITT methods, there is a significant advantage in Li-ion diffusion in W-modified NMC. These results could be ascribed to the existence of the compounds of Li, W and O like Li_xWO_3 or Li_2WO_4, which is a good lithium ion conductor [31,32,56]. Therefore, the W modification on NMC facilitate on Li-ion diffusion, reduce electrochemical polarization and improve the rate capability.

The EIS measurements were conducted to investigate the electrochemical resistance after charging to 4.5 V. Fig. 8(a) and (b) show Nyquist plots of pristine NMC electrodes and NMC-3%W after different cycles. The plots at an enlarged scale are shown in the insets. The spectra of each electrode can be regarded as the combination of two semicircles when the coin cells are charged to 4.5 V under 0.5C. The intercept at high frequency is R_{sol} corresponding to the uncompensated ohmic resistance of solution resistance. The small semicircle is R_{sf} caused by coating layer and the solid electrolyte interface (SEI). The other semicircle at low frequency is the charge transfer resistance (R_{ct}). Additionally, the inclined line at low frequency is corresponding to Warburg impedance Z_w, which is related to Lithium ion diffusion in electrode materials [57–60]. The corresponding equivalent circuit model of EIS fitting is shown in Fig. 8(c). Table 3 shows the resistance values calculated by the equivalent circuit model. The results show that R_{ct} of pristine NMC increases less than that of NMC-3%W electrode with the cycling. The R_{ct} of NMC-3%W electrode is 73.27 Ω after 100 cycles, which is only one tenth of the value (731Ω) of pristine NMC electrode. The results are attributed to the presence of WO_3 which scavenge HF, inhibit NMC/electrolyte interfacial reactions and reduce interfacial resistance. It is noticed that R_{sf} for both pristine NMC and NMC-3%W decrease in the initial several cycles, and then increase in subsequent cycles. Even so, R_{sf} still keeps at a low value after 100 cycles. The decrease of R_{sf} is attributed to NMC activation during the initial cycles and the SEI formation, while the increase of R_{sf} could be ascribed to the growth of SEI layer with the cycles. Furthermore, the sum of R_{sf} and R_{ct} are compared in Fig. 8(d). The NMC-3%W electrode has a lower sum of R_{sf} and R_{ct} than pristine NMC electrode, which can explain that NMC-3%W samples have the better rate performance.

4. Conclusions

In present studies, the tungsten-modified $LiNi_{1/3}Co_{1/3}Mn_{1/3}O_2$ cathode materials are successfully prepared through a facile and low cost ball-milling and annealing process. The tungsten compounds outside NMC particle retard the cathode/electrolyte interfacial reactions and facilitate ion diffusion in the batteries. After 100 cycles at 0.5C rate in 3–4.5 V range, NMC-3%W sample maintains 162 mAh g^{-1} discharge capacity with an improved capacity retention of 96% (representing 16% increase). After 100 cycles at 1C rate, NMC-3%W sample delivers 145 mAh g^{-1} discharge capacity with 16% increase. Moreover, the tungsten compounds also improve the rate capacity of the NMC cathode. The discharge capacity of NMC-3%W achieves to 123 mAh g^{-1} at 10C, which increase 57.6% than that of pristine NMC. Li-ion diffusion property investigated by CV and GITT methods indicates that tungsten compounds enhance apparent Li-ion diffusion in cathode and reduce electrochemical polarization. EIS results prove that the tungsten compounds impede cathode/electrolyte interfacial reactions, resulting in the decreases of charge transfer resistance and capacity degradation.

Acknowledgments

This work is supported partially by Natural Science Foundation of Beijing Municipality (L172036), Joint Funds of the Equipment Pre-Research and Ministry of Education (6141A020225), Par-Eu Scholars Program, Science and Technology Beijing 100 Leading Talent Training Project, Beijing Municipal Science and Technology Project (Z161100002616039), the Fundamental Research Funds for the Central Universities (2016JQ01, 2017ZZD02) and the NCEPU "Double First-Class" Graduate Talent Cultivation Program.

Appendix A. Supplementary data

Supplementary data to this article can be found online at https://doi.org/10.1016/j.electacta.2018.11.202.

References

[1] A.S. Arico, P. Bruce, B. Scrosati, J.-M. Tarascon, W. Van Schalkwijk, Nanostructured materials for advanced energy conversion and storage devices, Nat. Mater. 4 (2005) 366.
[2] B. Dunn, H. Kamath, J.-M. Tarascon, Electrical energy storage for the grid: a battery of choices, Science 334 (2011) 928–935.
[3] D. Larcher, J.-M. Tarascon, Towards greener and more sustainable batteries for electrical energy storage, Nat. Chem. 7 (2015) 19.
[4] S. Hy, H. Liu, M. Zhang, D. Qian, B.-J. Hwang, Y.S. Meng, Performance and design considerations for lithium excess layered oxide positive electrode materials for lithium ion batteries, Energy Environ. Sci. 9 (2016) 1931–1954.
[5] X. Li, Y. Feng, M. Li, W. Li, H. Wei, D. Song, Smart hybrids of Zn_2GeO_4 nanoparticles and ultrathin g-C_3N_4 layers: synergistic lithium storage and excellent electrochemical performance, Adv. Funct. Mater. 25 (2015) 6858–6866.
[6] M.D. Radin, S. Hy, M. Sina, C. Fang, H. Liu, J. Vinckeviciute, M. Zhang, M.S. Whittingham, Y.S. Meng, A.V.d. Ven, Narrowing the gap between theoretical and practical capacities in Li-ion layered oxide cathode materials, Adv. Energy Mater. 7 (2017), 1602888.
[7] H. Liu, H. Liu, S.H. Lapidus, Y.S. Meng, P.J. Chupas, K.W. Chapman, Sensitivity and limitations of structures from X-ray and neutron-based diffraction analyses of transition metal oxide lithium-battery electrodes, J. Electrochem. Soc. 164 (2017) A1802–A1811.
[8] J. Xu, H.D. Liu, Y.S. Meng, Exploring Li substituted O3-structured layered oxides $NaLi_xNi_{1/3-x}Mn_{1/3+x}Co_{1/3-x}O_2$ (x=0.07, 0.13, and 0.2) as promising cathode materials for rechargeable Na batteries, Electrochem. Commun. 60 (2015) 13–16.
[9] P. Cui, B. Xie, X. Li, M. Li, Y. Li, Y. Wang, Z. Liu, X. Liu, J. Huang, D. Song, J.M. Mbengue, Anatase/TiO_2-B hybrid microspheres constructed from ultrathin nanosheets: facile synthesis and application for fast lithium ion storage, CrystEngComm 17 (2015) 7930–7937.
[10] L. Chu, M. Li, Z. Wan, L. Ding, D. Song, S. Dou, J. Chen, Y. Wang, Morphology control and fabrication of multi-shelled NiO spheres by tuning the pH value via a hydrothermal process, CrystEngComm 16 (2014) 11096–11101.
[11] N.W. Li, X. Du, J.L. Shi, X. Zhang, W. Fan, J. Wang, S. Zhao, Y. Liu, W. Xu, M. Li, Y.G. Guo, C. Li, Graphene@hierarchical meso-/microporous carbon for ultrahigh energy density lithium-ion capacitors, Electrochim. Acta 281 (2018) 459–465.
[12] T. Ohzuku, Y. Makimura, Layered lithium insertion material of $LiNi_{1/2}Mn_{1/2}O_2$: a possible alternative to $LiCoO_2$ for advanced lithium-ion batteries, Chem. Lett. 30 (2001) 744–745.
[13] Z. Lu, D. MacNeil, J. Dahn, Layered $Li[Ni_xCo_{1-2x}Mn_x]O_2$ cathode materials for lithium-ion batteries, Electrochem. Solid State Lett. 4 (2001) A200–A203.
[14] P.-E. Cabelguen, D. Peralta, M. Cugnet, P. Maillet, Impact of morphological changes of $LiNi_{1/3}Mn_{1/3}Co_{1/3}O_2$ on lithium-ion cathode performances, J. Power Sources 346 (2017) 13–23.
[15] H.-J. Noh, S. Youn, C.S. Yoon, Y.-K. Sun, Comparison of the structural and electrochemical properties of layered $Li[Ni_xCo_yMn_z]O_2$ (x=1/3, 0.5, 0.6, 0.7, 0.8 and 0.85) cathode material for lithium-ion batteries, J. Power Sources 233 (2013) 121–130.
[16] S.K. Jung, H. Gwon, J. Hong, K.Y. Park, D.H. Seo, H. Kim, J. Hyun, W. Yang, K. Kang, Understanding the degradation mechanisms of $LiNi_{0.5}Co_{0.2}Mn_{0.3}O_2$ cathode material in lithium ion batteries, Adv. Energy Mater. 4 (2014), 1300787.
[17] H. Liu, H. Liu, I.D. Seymour, N. Chernova, K.M. Wiaderek, N.M. Trease, S. Hy,

Y. Chen, K. An, M. Zhang, O.J. Borkiewicz, S.H. Lapidus, B. Qiu, Y. Xia, Z. Liu, P.J. Chupas, K.W. Chapman, M.S. Whittingham, C.P. Grey, Y.S. Meng, Identifying the chemical and structural irreversibility in $LiNi_{0.8}Co_{0.15}Al_{0.05}O_2$ - a model compound for classical layered intercalation, J. Mater. Chem. A 6 (2018) 4189–4198.

[18] N.M. Trease, I.D. Seymour, M.D. Radin, H. Liu, H. Liu, S. Hy, N. Chernova, P. Parikh, A. Devaraj, K.M. Wiaderek, P.J. Chupas, K.W. Chapman, M.S. Whittingham, Y.S. Meng, A. Van der Van, C.P. Grey, Identifying the distribution of Al^{3+} in $LiNi_{0.8}Co_{0.15}Al_{0.05}O_2$, Chem. Mater. 28 (2016) 8170–8180.

[19] D. Li, Y. Kato, K. Kobayakawa, H. Noguchi, Y. Sato, Preparation and electrochemical characteristics of $LiNi_{1/3}Mn_{1/3}Co_{1/3}O_2$ coated with metal oxides coating, J. Power Sources 160 (2006) 1342–1348.

[20] J. Huang, H. Liu, T. Hu, Y.S. Meng, J. Luo, Enhancing the electrochemical performance of Li-rich layered oxide $Li_{1.13}Ni_{0.3}Mn_{0.57}O_2$ via WO_3 doping and accompanying spontaneous surface phase formation, J. Power Sources 375 (2018) 21–28.

[21] J. Huang, H. Liu, N. Zhou, K. An, Y.S. Meng, J. Luo, Enhancing the ion transport in $LiMn_{1.5}Ni_{0.5}O_4$ by altering the particle wulff shape via anisotropic surface segregation, ACS Appl. Mater. Interfaces 9 (2017) 36745–36754.

[22] S.J. Shi, J.P. Tu, Y.Y. Tang, Y.Q. Zhang, X.Y. Liu, X.L. Wang, C.D. Gu, Enhanced electrochemical performance of LiF-modified $LiNi_{1/3}Co_{1/3}Mn_{1/3}O_2$ cathode materials for Li-ion batteries, J. Power Sources 225 (2013) 338–346.

[23] H. Liu, D. Qian, M.G. Verde, M. Zhang, L. Baggetto, K. An, Y. Chen, K.J. Carroll, D. Lau, M. Chi, G.M. Veith, Y.S. Meng, Understanding the role of NH_4F and Al_2O_3 surface Co-modification on lithium-excess layered oxide $Li_{1.2}Ni_{0.2}Mn_{0.6}O_2$, ACS Appl. Mater. Interfaces 7 (2015) 19189–19200.

[24] S.-W. Lee, M.-S. Kim, J.H. Jeong, D.-H. Kim, K.Y. Chung, K.C. Roh, K.-B. Kim, Li_3PO_4 surface coating on Ni-rich $LiNi_{0.6}Co_{0.2}Mn_{0.2}O_2$ by a citric acid assisted sol-gel method: improved thermal stability and high-voltage performance, J. Power Sources 360 (2017) 206–214.

[25] H.D. Liu, J.J. Huang, D.N. Qian, S. Hy, C.C. Fang, J. Luo, Y.S. Meng, Communication-Enhancing the electrochemical performance of lithium-excess layered oxide $Li_{1.13}Ni_{0.3}Mn_{0.57}O_2$ via a facile nanoscale surface modification, J. Electrochem. Soc. 163 (2016) A971–A973.

[26] Y. Shi, M. Zhang, D. Qian, Y.S. Meng, Ultrathin Al_2O_3 coatings for improved cycling performance and thermal stability of $LiNi_{0.5}Co_{0.2}Mn_{0.3}O_2$ cathode material, Electrochim. Acta 203 (2016) 154–161.

[27] Y. Zhang, Z.-B. Wang, F.-D. Yu, L.-F. Que, M.-J. Wang, Y.-F. Xia, Y. Xue, J. Wu, Studies on stability and capacity for long-life cycle performance of $Li(Ni_{0.5-Co_{0.2}Mn_{0.3}})O_2$ by Mo modification for lithium-ion battery, J. Power Sources 358 (2017) 1–12.

[28] L. Gao, F. Qu, X. Wu, Hierarchical WO_3@SnO_2 core–shell nanowire arrays on carbon cloth: a new class of anode for high-performance lithium-ion batteries, J. Mater. Chem. A 2 (2014) 7367–7372.

[29] W. Wang, X. Meng, K. Zhang, P. Li, D. Choi, J.H. Park, Y. Son, Hollow and yolk-shell structured off-stoichiometric tungsten trioxide via selective leaching and hydrogenation for enhanced lithium storage properties, Electrochim. Acta 215 (2016) 466–472.

[30] M. Aykol, S. Kim, V.I. Hegde, D. Snydacker, Z. Lu, S. Hao, S. Kirklin, D. Morgan, C. Wolverton, High-throughput computational design of cathode coatings for Li-ion batteries, Nat. Commun. 7 (2016) 13779.

[31] T. Hayashi, T. Miyazaki, Y. Matsuda, N. Kuwata, M. Saruwatari, Y. Furuichi, K. Kurihara, R. Kuzuo, J. Kawamura, Effect of lithium-ion diffusibility on interfacial resistance of $LiCoO_2$ thin film electrode modified with lithium tungsten oxides, J. Power Sources 305 (2016) 46–53.

[32] T. Hayashi, J. Okada, E. Toda, R. Kuzuo, Y. Matsuda, N. Kuwata, J. Kawamura, Electrochemical effect of lithium tungsten oxide modification on $LiCoO_2$ thin film electrode, J. Power Sources 285 (2015) 559–567.

[33] B. Qiu, M. Zhang, L. Wu, J. Wang, Y. Xia, D. Qian, H. Liu, S. Hy, Y. Chen, K. An, Y. Zhu, Z. Liu, Y.S. Meng, Gas–solid interfacial modification of oxygen activity in layered oxide cathodes for lithium-ion batteries, Nat. Commun. 7 (2016) 12108.

[34] M.G. Verde, H.D. Liu, K.J. Carroll, L. Baggetto, G.M. Veith, Y.S. Meng, Effect of morphology and manganese valence on the voltage fade and capacity retention of $Li[Li_{2/12}Ni_{3/12}Mn_{7/12}]O_2$, ACS Appl. Mater. Interfaces 6 (2014) 18868–18877.

[35] H.-D. Lim, H.-K. Lim, X. Xing, B.-S. Lee, H. Liu, C. Coaty, H. Kim, P. Liu, Solid electrolyte layers by solution deposition, Adv. Mater. Interfaces 5 (2018), 1701328.

[36] H.-D. Lim, X. Yue, X. Xing, V. Petrova, M. Gonzalez, H. Liu, P. Liu, Designing solution chemistries for the low-temperature synthesis of sulfide-based solid electrolytes, J. Mater. Chem. A 6 (2018) 7370–7374.

[37] H. Liu, Y. Chen, S. Hy, K. An, S. Venkatachalam, D. Qian, M. Zhang, Y.S. Meng, Operando lithium dynamics in the Li-rich layered oxide cathode material via neutron diffraction, Adv. Energy Mater. 6 (2016), 1502143.

[38] H.D. Liu, C.R. Fell, K. An, L. Cai, Y.S. Meng, In-situ neutron diffraction study of the $xLi_2MnO_3.(1-x)LiMO_2$ (x= 0, 0.5; M= Ni, Mn, Co) layered oxide compounds during electrochemical cycling, J. Power Sources 240 (2013) 772–778.

[39] H.D. Liu, J. Xu, C.Z. Ma, Y.S. Meng, A new O3-type layered oxide cathode with high energy/power density for rechargeable Na batteries, Chem. Commun. 51 (2015) 4693–4696.

[40] H. Liu, H. Liu, S.H. Lapidus, Y.S. Meng, P.J. Chupas, K.W. Chapman, Sensitivity and limitations of Structures from X-ray and neutron-based diffraction analyses of transition metal oxide lithium-battery electrodes, J. Electrochem. Soc. 164 (2017) A1802–A1811.

[41] D. Lv, L. Wang, P. Hu, Z. Sun, Z. Chen, Q. Zhang, W. Cheng, W. Ren, L. Bian, J. Xu, A. Chang, Li_2O-B_2O_3-Li_2SO_4 modified $LiNi_{1/3}Co_{1/3}Mn_{1/3}O_2$ cathode material for enhanced electrochemical performance, Electrochim. Acta 247 (2017) 803–811.

[42] D. Li, Y. Sasaki, M. Kageyama, K. Kobayakawa, Y. Sato, Structure, morphology and electrochemical properties of $LiNi_{0.5}Mn_{0.5-x}Co_xO_2$ prepared by solid state reaction, J. Power Sources 148 (2005) 85–89.

[43] T. Aida, Y. Tsutsui, S. Kanada, J. Okada, K. Hayashi, T. Komukai, Ammonium tungstate modified Li-rich $Li_{1+x}Ni_{0.35}Co_{0.35}Mn_{0.30}O_2$ to improve rate capability and productivity of lithium-ion batteries, J. Solid State Electrochem. 21 (2017) 2047–2054.

[44] J.-N. Zhang, Q.-H. Li, Q. Li, X.-Q. Yu, H. Li, Improved electrochemical performances of high voltage $LiCoO_2$ with tungsten doping, Chin. Phys. B 27 (2018), 088202.

[45] A. Enesca, C. Enache, A. Duta, J. Schoonman, High crystalline tungsten trioxide thin layer obtained by SPD technique, J. Eur. Ceram. Soc. 26 (2006) 571–576.

[46] A.P. Shpak, A.M. Korduban, M.M. Medvedskij, V.O. Kandyba, XPS studies of active elements surface of gas sensors based on WO_{3-x} nanoparticles, J. Electron. Spectrosc. Relat. Phenom. 156–158 (2007) 172–175.

[47] P. Li, X. Li, Z. Zhao, M. Wang, T. Fox, Q. Zhang, Y. Zhou, Correlations among structure, composition and electrochemical performances of WO_3 anode materials for lithium ion batteries, Electrochim. Acta 192 (2016) 148–157.

[48] Y.K. Sun, S.T. Myung, B.C. Park, J. Prakash, I. Belharouak, K. Amine, High-energy cathode material for long-life and safe lithium batteries, Nat. Mater. 8 (2009) 320–324.

[49] S. Park, C. Yoon, S. Kang, H.-S. Kim, S.-I. Moon, Y.-K. Sun, Synthesis and structural characterization of layered Li $[Ni_{1/3}Co_{1/3}Mn_{1/3}]O_2$ cathode materials by ultrasonic spray pyrolysis method, Electrochim. Acta 49 (2004) 557–563.

[50] Z. Wu, S. Ji, T. Liu, Y. Duan, S. Xiao, Y. Lin, K. Xu, F. Pan, Aligned Li^+ tunnels in core-shell $Li(Ni_xMn_yCo_z)O_2$@$LiFePO_4$ enhances its high voltage cycling stability as Li-ion battery cathode, Nano Lett. 16 (2016) 6357–6363.

[51] L.L. Zhang, J.Q. Wang, X.L. Yang, G. Liang, T. Li, P.L. Yu, D. Ma, Enhanced electrochemical performance of fast ionic conductor $LiTi_2(PO_4)_3$-coated $LiNi_{1/3}Co_{1/3}Mn_{1/3}O_2$ cathode material, ACS Appl. Mater. Interfaces 10 (2018) 11663–11670.

[52] D. Jin, D. Song, A. Friesen, Y.M. Lee, M.-H. Ryou, Effect of Al_2O_3 ceramic fillers in $LiNi_{1/3}Co_{1/3}Mn_{1/3}O_2$ cathodes for improving high-voltage cycling and rate capability performance, Electrochim. Acta 259 (2018) 578–586.

[53] Y. Denis, C. Fietzek, W. Weydanz, K. Donoue, T. Inoue, H. Kurokawa, S. Fujitani, Study of $LiFePO_4$ by cyclic voltammetry, J. Electrochem. Soc. 154 (2007) A253–A257.

[54] Y. Wei, J. Zheng, S. Cui, X. Song, Y. Su, W. Deng, Z. Wu, X. Wang, W. Wang, M. Rao, Y. Lin, C. Wang, K. Amine, F. Pan, Kinetics tuning of Li-ion diffusion in layered $Li(Ni_xMn_yCo_z)O_2$, J. Am. Chem. Soc. 137 (2015) 8364–8367.

[55] A.J. Bard, L.R. Faulkner, Electrochemical Methods: Fundamentals and Applications, second ed., Wiley, New York, 2001.

[56] T. Hayashi, Y. Matsuda, N. Kuwata, J. Kawamura, High-power durability of $LiCoO_2$ thin film electrode modified with amorphous lithium tungsten oxide, J. Power Sources 354 (2017) 41–47.

[57] X.Y. Qiu, Q.C. Zhuang, Q.Q. Zhang, R. Cao, Y.H. Qiang, P.Z. Ying, S.G. Sun, Investigation of layered $LiNi_{1/3}Co_{1/3}Mn_{1/3}O_2$ cathode of lithium ion battery by electrochemical impedance spectroscopy, J. Electroanal. Chem. 687 (2012) 35–44.

[58] L. Chu, M. Li, X. Li, Y. Wang, Z. Wan, S. Dou, D. Song, Y. Li, B. Jiang, High performance NiO microsphere anode assembled from porous nanosheets for lithium-ion batteries, RSC Adv. 5 (2015) 49765–49770.

[59] G. Wu, J. Chen, Y. Guo, X. Li, B. Luo, L. Chu, Y. Han, B. Jiang, L. Xu, M. Li, Freestanding sodium-ion batteries electrode using graphene foam coaxially integrated with TiO_2 nanosheets, J. Electrochem. Soc. 164 (2017) A3060–A3067.

[60] B.S. Lee, Z. Wu, V. Petrova, X. Xing, H.D. Lim, H. Liu, P. Liu, Analysis of rate-limiting factors in thick electrodes for electric vehicle applications, J. Electrochem. Soc. 165 (2018) A525–A533.